

Title: Atrial-specific upregulation of miR-31 in human atrial fibrillation begets the arrhythmia by depleting dystrophin and neuronal nitric oxide synthase.

One Sentence Summary: Atrial myocyte-specific upregulation of microRNA-31 in human atrial fibrillation causes dystrophin and nNOS depletion, which, in turn, contributes to the electrical phenotype begetting the arrhythmia.

Svetlana N Reilly, MD, DPhil ^{1*}, Xing Liu, PhD ^{1*}, Ricardo Carnicer, PhD ¹, Alice Recalde, PhD ¹, Anna Muszkiewicz MChemPhys², Raja Jayaram, MD ¹, Maria Cristina Carena BSc ¹, Rohan Wijesurenda, MB BChir, MRCP ¹, Matilde Stefanini BSc MSc¹, Nicoletta C. Surdo, PhD ¹, Oliver Lomas, BM BCh, MRCP ¹, Chandi Ratnatunga, FRCS ³, Rana Sayeed, PhD, FRCS ³, George Krasopoulos, PhD, FRCS ³, Timothy Rajakumar BSc ⁴, Alfonso Bueno-Orovio PhD ², Sander Verheule, PhD ⁵, Tudor A. Fulga, PhD ⁴, Blanca Rodriguez PhD², Ulrich Schotten MD, PhD ⁵, Barbara Casadei, MD, DPhil, FRCP, FMedSci ¹.

¹ Division of Cardiovascular Medicine, Radcliffe Department of Medicine, University of Oxford, John Radcliffe Hospital, UK

² Department of Computer Science, University of Oxford, UK

³ Department of Physiology, University of Maastricht, The Netherlands

⁴ Weatherall Institute of Molecular Medicine, Radcliffe Department of Medicine, University of Oxford, UK

* These authors have contributed equally to the manuscript.

Address correspondence to:

Prof Barbara Casadei or Dr Svetlana Reilly
Division of Cardiovascular Medicine
Radcliffe Department of Medicine
University of Oxford
Level 6, West Wing
John Radcliffe Hospital
OX3 9DU
UK

Tel. +44 (0)1865 234 664/660

Fax. +44 (0)1865 234 667

E-mail: barbara.casadei@cardiov.ox.ac.uk

E-mail: svetlana.reilly@cardiov.ox.ac.uk

Total word count (including references): 8,011

Abstract: Atrial fibrillation (AF) is a growing public health burden and its treatment remains a challenge. AF leads to electrical remodeling of the atria, which, in turn, promotes AF maintenance and resistance to treatment. Although remodeling has long been a therapeutic target in AF, its causes remain poorly understood. Here we show that atrial-specific upregulation of microRNA 31 (miR-31) in goat and human AF depletes neuronal nitric oxide synthase (nNOS) by accelerating mRNA decay and alters nNOS subcellular localization by repressing dystrophin translation. By shortening action potential duration (APD) and abolishing APD rate-dependent adaptation, miR-31 overexpression and/or disruption of nNOS signaling recapitulate features of AF-induced remodeling and significantly increase AF inducibility in mice *in vivo*. By contrast, silencing miR-31 in atrial myocytes from patients with AF restores dystrophin and nNOS and normalizes APD and its rate-dependency. These findings identify atrial-specific upregulation of miR-31 in human AF as a key mechanism causing atrial dystrophin and nNOS depletion, which, in turn, contributes to the atrial phenotype begetting this arrhythmia.

Key words: neuronal nitric oxide synthase; dystrophin; atrial fibrillation; microRNA

INTRODUCTION

Atrial fibrillation (AF) is the most common heart rhythm disorder worldwide and a major public health burden due to its impact on the risk of stroke and heart failure (1). The last 20 years have witnessed a significant increase in the incidence of AF in the developed and developing world caused by population ageing and the rising prevalence of risk factors for AF, such as hypertension, obesity and diabetes (2). Pharmacological strategies to restore sinus rhythm (SR) in patients with AF have been marred by poor efficacy and safety concerns related to their propensity to induce life-threatening ventricular arrhythmias (3). Similarly, whether AF ablation techniques have long-lasting effects on the restoration of SR and a beneficial impact on patient outcomes remains to be demonstrated (1). Underlying AF resistance to treatment, is the ability of the arrhythmia to sustain itself by inducing electrical and structural remodeling of the atria, which, in turn, promotes AF maintenance and increases vulnerability to relapse (4). The mechanisms leading to atrial remodeling in AF are poorly understood and identification of atrial-specific molecular targets upstream of this process has been focus of intense investigation.

Nitric oxide (NO) is known to regulate atrial electrical properties (5) and exert anti-fibrotic and anti-thrombotic actions (6). Short-term AF has been reported to induce a profound reduction in atrial NO release in animal models and inconsistent changes in the “endothelial” isoform of NO synthase (eNOS) (6, 7). A “neuronal” NOS isoform (nNOS) is also constitutively expressed in the sarcoplasmic reticulum and sarcolemmal membrane of cardiomyocytes (as part of the dystrophin-associated glycoprotein complex (8)) where nNOS-derived NO regulates sarcolemmal ion conductance (5) and calcium fluxes under basal conditions and in response to mechanical stress and prevents arrhythmic death in mice after myocardial infarction (9, 10). Basal blood flow in the human coronary vascular bed and perfusion of the exercising muscle are also regulated by nNOS-derived NO (11, 12) and loss of sarcolemmal nNOS in the skeletal muscle of patients with Duchenne muscular dystrophy (DMD) (13) leads the dystrophin-deficient muscle to ischemia during contraction (14), suggesting that subcellular localization of nNOS signaling may be an important function of the dystrophin-associated glycoprotein complex.

Here we show that atrial-specific upregulation of microRNA-31 (miR-31) in goats and patients with AF leads to nNOS depletion (by accelerating nNOS mRNA decay) and disrupts nNOS sarcolemmal localization by translational repression of dystrophin, resulting in loss of sarcolemmal nNOS and a profound reduction in NOS activity. By shortening APD and abolishing APD rate-dependent adaptation, miR-31 overexpression and disruption of nNOS signaling contribute to the AF-induced electrical remodeling of the atrial myocardium and significantly increase AF inducibility *in vivo* in mice.

RESULTS

To address whether changes in atrial nNOS expression and activity are an early event in the natural history of AF, we examined samples of atrial tissue from 51 patients with persistent AF and 165 controls in sinus rhythm (SR) (**Table 1**), and from goats after 2 weeks (2W, n=11) or 6 months (6M, n=9) of pacing-induced AF (vs. 16 control in SR). NOS activity and nNOS protein content were substantially lower in the presence of AF in all groups, whereas other NOS isoforms did not change significantly (**Fig. 1A-D & Fig. S1A-C**).

We then evaluated whether nNOS deficiency alters the electrical properties of human and murine right atrial myocytes. nNOS gene deletion or inhibition with S-methylthiocitrulline (SMTC, 100 nmol/L) did not affect the resting membrane potential or the action potential (AP) amplitude (**Table S1**) but significantly reduced APD at 50% and 90% of repolarization (**Fig. 1E**) and abolished the APD's rate-dependent adaptation in atrial myocytes from patients in SR (**Fig. 1F**), but had no effect in the presence of AF. A shorter APD was also observed in atrial myocytes from nNOS^{-/-} mice, in wild type (WT) myocytes upon nNOS inhibition with SMTC (**Fig. 1G**), and in human atrial myocytes after nNOS knockdown by siRNA (**Fig S2A-C**). These findings mimic the hallmark features of AF-induced electrical remodelling, which, by facilitating functional re-entry, promotes induction and maintenance of AF (4).

Nitric oxide has been shown to regulate a number of sarcolemmal ion currents both *via* cyclic GMP-mediated changes in phosphorylation and by S-nitrosation of the channel protein (5). In right atrial myocytes from patients in SR, nNOS inhibition resulted in a significant increase in the atrial-specific ultra-rapid delayed rectifier K⁺ current (I_{Kur}) (**Fig. 2A, B**), the transient outward potassium current (I_{to}) (**Fig. S2D**), and the inward-rectifier K⁺ current (I_{K1}) (**Fig. 2C**), with a trend towards an increase in the L-type calcium current (I_{Ca} , +18.3%±15.1% at 20 mV, P=0.12, n=18-20 myocytes, N=12). The relative impact of these changes in ion current density on APD₅₀ and APD₉₀ was evaluated *in silico* using an experimentally-calibrated population of 640 human atrial cell models, sharing the same equations but with differences in ionic conductance and permeability (15). As shown in **Fig 2D, E**, mimicking the increase I_{Kur} induced by SMTC reproduced most of the reduction in APD₅₀ observed experimentally. Modeling the increase of both I_{Kur} and I_{K1} also recovered the reduction in APD₉₀ whereas the observed changes in I_{to} and I_{Ca} had no impact on APD. These findings were confirmed by experiments showing that inhibition of I_{Kur} using 4-aminopiridine (4-AP, 50 µmol/L (16)) abolished the effect of SMTC on APD in atrial myocytes from patients in SR (**Fig. S2E**).

To assess whether loss of nNOS is sufficient to provide a substrate for AF *in vivo*, we evaluated AF inducibility by performing atrial burst pacing (17) in nNOS^{-/-} mice and their WT littermates. As shown in **Fig. 2F**, AF inducibility and duration were significantly higher

in nNOS^{-/-} mice, in the absence of electrophysiological (**Table S2**) or structural cardiac abnormalities (9). Together, these findings indicate that reduced availability of nNOS-derived NO, as observed in the fibrillating human atrial myocardium, contributes to shorten atrial APD and is sufficient to increase AF inducibility *in vivo*.

We next investigated the mechanism responsible for nNOS depletion in the fibrillating human atrial myocardium. In skeletal muscle, nNOS is bound to the dystrophin-associated glycoprotein complex (18), the disruption of which leads to the near-disappearance of nNOS at the sarcolemmal membrane, as observed in DMD (13). **Figure 3A, C, D** shows that dystrophin and nNOS co-immunoprecipitate and co-localize to the sarcolemma of human atrial myocytes in SR, but not in AF, where dystrophin (evaluated by using both antibodies directed to the protein rod domain and the C-terminus, **Fig. 3B, E** and **Fig. S3C**, respectively) and its associated proteins (*e.g.*, caveolin-3 and 1 α syntrophin) are also significantly reduced (**Fig. 3E** and **Fig. S3A, B** in atrial goat tissue). By contrast, nNOS gene deletion does not alter atrial dystrophin content in mice (**Fig. S3D**).

As reported in the skeletal muscle of patients with DMD (19), we also observed a significant reduction in nNOS mRNA in atrial myocytes from patients with AF (**Fig. 3F**), whereas dystrophin mRNA (**Fig. 3G**) was unchanged.

To evaluate whether post-transcriptional regulation of atrial nNOS and dystrophin contributes to their depletion in human AF, we carried out an *in silico* analysis to identify microRNAs predicted to target both transcripts in humans. Amongst these, miR-31 had previously been reported to repress dystrophin translation in the skeletal muscle of patients with DMD (20). As shown in **Fig. 3H, I** and **Fig. S4A**, we observed a significant increase in miR-31 in atrial myocytes and tissue from patients and goats with AF but not in goat left ventricular tissue. By contrast, in patients with paroxysmal AF or in those who developed AF after cardiac surgery (**Tables S3 and S4**), atrial miR-31 was not upregulated nor was nNOS or dystrophin protein content decreased (compared with matched patients in SR or patients who remained in SR after cardiac surgery, respectively, **Fig. S5**), in keeping with evidence indicating that atrial electrical remodeling is not present in patients with paroxysmal AF nor does it precede the occurrence of AF (21).

Prediction algorithms identified one conserved putative miR-31 binding site on the human dystrophin 3' untranslated region (3'UTR) and five in the human nNOS 3'UTR (**Table S5**), only one of which (site 5) was shown to be functional in a reporter assay in HEK293T cells, which also confirmed functionality of the miR-31 binding site in the dystrophin 3'UTR (20) (**Fig. S6**).

mRNA regulation by small, non-coding miRs is accomplished through the RNA-induced silencing complex (RISC), where Argonaute proteins associated with miRs bind to the 3'-

UTR of mRNAs facilitating their degradation or inhibiting translation (22). In atrial myocytes from patients with AF, immunoprecipitation of Argonaute 2 (Ago2, **Fig. S7A**) confirmed the presence of nNOS and dystrophin mRNA within the RISC (**Fig. 4A, B**). Blocking the corresponding miR-31 binding site with a selective locked-nucleic acid (LNA)-enhanced miR-31 target site blocker (TSB, **Table S6**) reduced the RISC incorporation of the respective mRNA (**Fig. 4A-B**) but not of miR-31 (**Suppl. Fig. 7B**).

To investigate the mode by which miR-31 regulates dystrophin and nNOS gene expression, their corresponding mRNA stability was assessed in the presence of a miR-31 mimic in human SR myocytes treated with the transcription inhibitor, actinomycin D. Under these conditions, miR-31 accelerated the decay of nNOS mRNA but not of dystrophin (**Fig. 4C, D** and **Fig. S7C, D**). In agreement with these findings, preventing the binding of miR-31 to nNOS mRNA in AF myocytes using a selective TSB, increased nNOS mRNA and partially recovered nNOS protein without affecting dystrophin mRNA and protein content (**Fig. 4E, F**). By contrast, preventing binding of miR-31 to dystrophin mRNA did not change nNOS or dystrophin mRNA but restored dystrophin protein content and partially recovered nNOS (**Fig. 4G, H**), indicating that dystrophin affects nNOS protein stability as well as its subcellular localization.

Together, these data confirm that miR-31 binds to the 3'UTR region of both dystrophin and nNOS mRNA in human atrial myocytes where it leads to a reduction of the respective protein by accelerating nNOS mRNA decay and inhibiting the translation of dystrophin mRNA.

We then evaluated whether miR-31 inhibition reversed the electrical phenotype observed in atrial myocytes from patients with AF. As shown in **Figure 5A, B** restoration of dystrophin and nNOS protein content in atrial myocytes from patients with AF following miR-31 inhibition (**Fig. S4B**) also restored APD and APD rate-dependent adaptation (**Fig. 5E, F**); both effects were reversed by nNOS inhibition, confirming that the effects of miR-31 on the electrical phenotype of human atrial myocytes are mediated by NO.

MiR-31 inhibition had no measurable effect on miR-31 expression, dystrophin or nNOS in atrial myocytes from patients in SR (**Fig. S4B, Fig. 5C, D**); however, in these cells, increasing intracellular miR-31 levels (by using a miR-31 mimic) reduced dystrophin and nNOS and lead to APD shortening and loss of APD rate-dependent adaptation (**Fig. S7E-I**).

DISCUSSION

AF is a self-promoting arrhythmia; paroxysmal AF frequently progresses to sustained AF and interventions aimed at recovering SR are less likely to succeed the longer AF lasts (1). An important advance in our understanding of AF has been the recognition that, by remodeling atrial electrical and structural properties, AF promotes its stabilization and progression and

confers resistance to treatment (4). Changes in the expression of genes encoding sarcolemmal ion channels contribute to AF-induced atrial remodeling and miRs have previously been reported to target the expression of ion channels subunits involved in this process (23). We have identified myocardial nNOS depletion as a novel molecular mechanism upstream of the atrial electrical substrate that sustains AF in humans. Upregulation of miR-31 in the human atrial myocardium is an early event in the natural history of AF that results in a profound reduction in atrial NO synthesis by accelerating nNOS mRNA decay, and repressing dystrophin translation, leading to altered nNOS subcellular localization and increased protein instability.

By reducing S-nitrosation (and increasing activity) of Class II histone deacetylase, nNOS depletion plays an important role in the epigenetic regulation of gene expression in DMD, contributing to muscle redox imbalance and injury (24). Indeed, increased oxidative stress is a common feature of the dystrophic heart muscle (25), the fibrillating human atrial myocardium (26) and the myocardium of nNOS^{-/-} mice (27). nNOS depletion or inhibition has been linked to muscle impaired perfusion (11, 14), and reduced dystrophin to altered Ca²⁺ homeostasis, increased membrane fragility, and cell death (25), suggesting that atrial nNOS/dystrophin depletion secondary to miR-31 upregulation impacts on all aspects of AF-induced atrial remodeling.

The effects of miR-31 upregulation on the atrial electrical phenotype are dependent on nNOS-derived NO and reproduced in atrial myocytes from the nNOS^{-/-} mouse, which show no difference in dystrophin content, suggesting that the latter has no direct impact on atrial AP characteristics. Although involvement of miR-31 in the downregulation of ion channels subunits in human AF cannot be excluded, APD shortening and loss of APD rate-dependent adaptation are detected following nNOS inhibition or knock-down in atrial myocytes from patients in SR and WT mice, indicating that constitutive myocardial NO production can rapidly modulate a number of sarcolemmal ion currents, as suggested by investigations employing NO donors (5). The latter, however, do not consistently reproduce the effects of NO released by constitutive NOS isoforms (28, 29), as subcellular localization is a critical determinant of myocardial NO signaling (9, 10). Similarly, acute nNOS inhibition does not mimic all the changes in atrial ion currents described in long-standing persistent AF, where I_{Ca} and I_{to} are substantially decreased, I_{Kur} is reduced or unchanged, and I_{K1} is increased (30). *In silico* modeling indicates that the increase in I_{Kur} and I_{K1} accounts for most of the effect of nNOS inhibition on APD₅₀ and APD₉₀ in human atrial myocytes, whereas the impact of the relatively small rise in I_{Ca} and I_{to} on APD is negligible.

Taken together, our findings suggest that atrial nNOS depletion in the early stages of AF favors the stabilization of the arrhythmia by shortening atrial refractoriness before changes in

protein content of ion channels subunits ensue. As upregulation of miR-31 is atrial-specific and its effects on atrial electrical properties are rapidly reversible, interventions targeted to this pathway may provide an effective and safer therapeutic option for patients with AF. More advanced delivery strategies (*e.g.*, tissue-specific vectors and promoters) as well as the identification of mechanisms leading to atrial miR-31 upregulation by AF may circumvent the lack of cell-specific targeting that is currently a major drawback of miR manipulation for therapeutic purposes (31).

MATERIAL AND METHODS

Study Design

The aim of this study was to investigate the cause and impact of impaired atrial NO production on AF-induced electrical remodeling in humans. The explorative phase of the study was conducted using whole tissue homogenates from samples of the right atrial appendage obtained from patients undergoing cardiac surgery and findings were subsequently validated in human right atrial myocytes. Time and chamber-specific trends in the reduction of nNOS activity/protein were explored in a goat model of pacing induced AF. Follow-up mechanistic studies were performed in isolated human atrial myocytes, goat atrial and ventricular tissue, and in nNOS^{-/-} mice and their wild type littermates. A total of 259 patients, 77 mice and 36 goats were included in the study. For ion current measurements, we used we used 3-6 atrial myocytes per patient/mice. Inhibitors and mimics were used to assess both the loss and gain of function of miR-31 on dystrophin and nNOS mRNA and protein content and on APD and APD rate-dependent adaptation in human atrial myocytes. *In vivo* studies were not randomized but experiments were carried out and analyzed with the operator blind of the genotype. No data were excluded.

Investigations were approved by local Research Ethics Committees or performed according to the European directive on laboratory animals (86/609/EEC) or the Home Office Guidance on the Operation of Animals (Scientific Procedures) Act, 1986. All patients gave informed written consent.

Goats. Female goats (weight, 45 to 61 kg) were instrumented, as described previously (32). AF was induced by repetitive burst pacing and maintained for 2 weeks (n=11) or 6 months (n=9); sham-operated goats in SR (n=16) were used as controls.

Mice. Homozygous mice (3-4 months old, N=37) with targeted disruption of nNOS (nNOS^{-/-}) were compared to their wild type littermates (WT, N=40).

All materials were purchased from Sigma (St. Louis, MO) unless specified.

NOS activity in human and goat atrial homogenates. Atrial NOS activity was evaluated by

conversion of [^{14}C]L-arginine to citrulline (in the presence of the arginase inhibitor N ω -hydroxy-nor-arginine, Calbiochem) by HPLC (26). Values are expressed as the N ω -Nitro-L-arginine methyl ester hydrochloride (L-NAME) - inhibitable fraction.

Immunoblotting in human, goat and murine atrial homogenates and in human atrial myocytes was performed as described previously (26). We used primary antibodies raised against nNOS (Santa Cruz Biotechnologies, USA), eNOS (BD Transduction Lab, USA), dystrophin (NCL-DYS1, rod domain and NCL-DYS2, C-terminus, Novocastra, Leica Biosystems, Germany, or Thermo Fisher Scientific, USA); Caveoline-3 and iNOS (Abcam, UK), α 1 syntrophin (Abd Serotec, USA), α -actinin, and GAPDH (Millipore, USA). Immunodetection of the primary antibodies was performed using horseradish-peroxidase conjugated secondary antibodies (Promega, USA), and normalized to GAPDH, unless specified. For some experiments, membrane and cytosolic fractions were separated by multiple centrifugation steps, as described previously (33).

Immunoprecipitation (IP) assay for dystrophin and nNOS in right atrial homogenates.

Atrial samples were homogenized on ice, centrifuged (15 min at 13,000 at 4°C), and immunoabsorbed with anti-nNOS or anti-dystrophin antibodies (NCL-DYS1). Immune complexes were precipitated for 3 hours by the addition of protein A/G-conjugated agarose (Santa Cruz), and immunoblotted with anti-nNOS and anti-dystrophin antibodies; agarose beads with Ig G/A alone were used as control for non-specific binding.

Immunostaining was performed in OCT-embedded cryosections of human atrial tissue, whereas co-localization between dystrophin and nNOS was evaluated in human atrial myocytes. Briefly, cryosections or myocytes were fixed in pre-cooled (-20°C) acetone: methanol (1:1) solution, air-dried and rinsed in phosphate buffered saline (PBS), blocked with serum-free blocking reagent (DAKO, Agilent Technologies, Denmark) and incubated with an anti-dystrophin or anti-nNOS antibody overnight at 4°C. Following multiple rinsing steps with 0.1% PBST, secondary Alexa Fluor antibodies (Invitrogen, USA) were applied for 1 hour at room temperature. Imaging was performed using a Zeiss LSM510 or Leica DM6000 CFS confocal imaging system.

Quantitative real-time PCR analysis. We compared the expression of dystrophin, nNOS and miR-31 transcripts using qPCR in human and goat cardiac tissue, or in human atrial myocytes. Briefly, total RNA was extracted with the miRNeasy kit (Qiagen) or miRvana kit (Applied Biosystems, USA) according to the manufacturer's instruction. RT-qPCR was carried out using the QuantiTect Reverse Transcription kit (Qiagen) and TaqMan Gene Expression Assays for dystrophin and nNOS (Applied Biosystems, USA; assay IDs: human dystrophin 3' region -, Hs01049460_m1, human dystrophin central domain - Hs00758098_m1, human dystrophin 5' region - Hs01049418_m1 & human nNOS -

Hs00167223_m1). For miR31 RT-qPCR, the TaqMan microRNA Reverse Transcription kit, TaqMan microRNA assay stem loop primers & TaqMan Universal Master Mix (all from Applied Biosystems, USA) were used.

For the gene expression assay on transfected human myocytes, a pre-amplification step was used prior to the qPCR, in accordance with the manufacturer's instruction. Each reaction was performed in duplicates using ABI 7900HT detection system (Applied Biosystems).

Relative quantification was obtained by using the comparative threshold cycle method ($2^{-\Delta\Delta Ct}$); the expression of the target gene was normalized to GAPDH or β -actin (for dystrophin and nNOS transcripts), or to snoU6 (for miR-31 expression) and related to a control reference sample.

Ribonucleoprotein immunoprecipitation (RIP) with Argonaute 2 (Ago2) in right atrial myocytes from patients with AF. The RIP assay was carried out to assess interaction between dystrophin or nNOS mRNA with miR-31 within the RNA-induced silencing complex (RISC). Human atrial myocytes were transfected for 48 hours with a LNA-based miR-31 TSB (20 nM) for dystrophin or nNOS, or the corresponding negative control (NC). RIP was performed using the Magna RIP kit (Millipore, USA). Briefly, cells were washed in PBS (x3) before lysis in 100 μ l complete RIP-lysis buffer and incubated with magnetic beads conjugated with anti-Ago2/eIF2C2 antibody (Abcam, UK) or rabbit IgG (Millipore, USA) and rotated overnight at 4°C. Co-immunoprecipitated RNA, including miR:mRNA complexes, was subjected to qPCR and miR-qPCR. Expression of dystrophin and nNOS genes was normalized to miR-31 and calculated using the comparative threshold cycle method ($2^{-\Delta\Delta Ct}$).

MiR-31 target predictions. Using 6 prediction algorithms, i.e., DIANAmt, miRanda, miRWalk, PICTAR5, PITA and Targetscan (for reference please refer to MiRWalk program: <http://www.umm.uni-heidelberg.de/apps/zmf/mirwalk/serverfull.php>), *in silico* analysis predicted binding of miR-31-5p to nNOS 3'UTR at 5 sites (**Table S5**).

Reporter assay. All reporter constructs were derived from pcDNATM3.1/Hygro(+) vector (Life Technologies). A dual fluorescence reporter (pCMV-dEGFP-SV40-ECFP) was generated by cloning the dEGFP gene into BamHI and NotI sites downstream of the CMV promoter, and by replacing the hygromycin resistance gene downstream of the SV40 promoter with ECFP using sequence-overlap extension PCR. A fragment of the dystrophin 3'UTR (~500 bp), or two fragments (named part 1 and part 2, ~500 bp each) of the nNOS 3'UTR, centered on each of the predicted miR-31 target binding sites, were cloned into the pCMV-dEGFP-SV40-ECFP vector. Site-directed mutagenesis (Mut) was used to create reporter constructs in which miR-31 target sites were individually or globally disrupted (**Fig. S6**). HEK293T cells were co-transfected with reporter constructs (250 ng) and miRIDIAN

miR-31 mimic (a double-stranded sequence of RNA oligonucleotides) or negative control #1 (10 nM – for nNOS sensor & 50 nM – for dystrophin sensor, both from Dharmacon) using a polyethylenimine transfection reagent (Invitrogen) in antibiotic-free DMEM containing 2% FBS. The effect of miR-31 on GFP fluorescence was measured by fluorescence-activated cell sorting (CyAn, DakoCytomation) 48 hours post-transfection. dEGFP was measured using a 488 nm laser and 530/40 nm emission filter. ECFP was measured using a 405 nm laser and 450/50 emission filter; ~50,000 events (for nNOS sensors) and ~20,000 (for the dystrophin sensors) were recorded per sample.

Isolation and culture of human atrial myocytes. Right and left atrial myocytes were isolated using a standard enzymatic dispersion technique, as described previously (34). Isolated cells were plated in 12-well plates freshly coated with 0.4 mg/ml laminin and cultured as described previously (35).

Transfection of human atrial myocytes. Atrial myocytes were transfected with (i) 20 nM miRIDIAN miR-31-5p hairpin inhibitor (α -miR-31, single-stranded RNA sequence) or 20 nM negative control #1 (based on cel-miR-67 sequence MIMAT0000039 which has no identity in the human genome); (ii) 10 nM miRIDIAN miR-31 (mature double-stranded RNA sequence) or negative control #1 (10 nM, all from Dharmacon); and (3) miR-31 LNA-based TSB on dystrophin or nNOS, or negative control (20 nM, Exiqon; all sequences are provided in **Table S6**), using the Opti-MEM medium, DharmaFECT 2 reagent (Dharmacon).

To knock-down nNOS, human atrial myocytes were transfected for ~80 hours with Accell siRNA SMARTpool generated for human nNOS (1 μ M) or with a respective non-targeting Accell control pool (1 μ M, both from Dharmacon) using Accell siRNA delivery media.

Transfection efficiency was evaluated by qRT-PCR with TaqMan miR-31 or gene expression assays (for nNOS and dystrophin, Applied Biosystems) and visually by using the miRIDIAN Dy547-labeled transfection control (for experiments with miR-31 mimic or inhibitor) or with Accell green non-targeting control in cells transfected with siRNA. 48-80 hours post-transfection, human atrial myocytes were harvested for patch clamping, immunoblotting, immunoprecipitation, RIP analysis or qPCR assay.

Transcription inhibition with actinomycin D. Atrial myocytes isolated from patients in SR were transfected with 10 nM of miRIDIAN miR-31 mimic (Dharmacon) for 24 hours and then treated with actinomycin D (5 μ g/ml) for 6 hours. Levels of the 3' region, central domain and 5' region of dystrophin mRNA and nNOS mRNA (qPCR) are shown as percentage of the respective mRNA at 0 hour, using GAPDH as the reference gene.

Electrophysiological recordings. Whole-cell voltage and current-clamp experiments were carried out in human and murine right atrial myocytes at 37°C (with the exception of I_{K1}) using an Axopatch 200B amplifier and Digidata 1322A data-acquisition system (Axon

Instruments). The electrode resistance ranged from 2-4 M Ω . After rupture of the membrane, membrane capacitance (C_m) was routinely measured, as described previously (36).

(i) Recording of APs using conventional whole-cell current clamp recording.

At least 25 steady-state APs were recorded at each cycle length. The AP amplitude and duration (at 50 and 90% of repolarization, APD_{50} and APD_{90}) were measured from the averaged traces. The pipette solution contained in mM: 130 K-Aspartate, 10 HEPES, 5 Na_2ATP , 2 $MgCl_2$, 5 $CaCl_2$, 11 EGTA (pH-7.2; pCa 7.0). Extracellular solution contained in mM: 140 NaCl, 5.4 KCl, 1.4 $CaCl_2$ (1.8 in human atrial myocytes), 1.2 $MgCl_2$, 10 glucose, 5 HEPES (pH-7.4).

(ii) Recording of K^+ currents.

To obtain current-voltage relationships of human right atrial I_{Kur} , currents were evoked by 500 ms steps from a holding potential of -70 mV to potentials ranging from -35 to $+45$ mV. A pre-pulse of 200 ms to -35 mV was applied to inactivate I_{Na} . I_{Kur} was obtained by digital subtraction of the current in the presence of 4-AP (50 μ mol/L) from I_{sus} (*i.e.*, the current at the end of the voltage step in the absence of 4-AP) (16).

I_{to} , was measured as the difference between the peak outward current and I_{sus} . Currents were evoked by 700 ms steps from a holding potential of -70 mV to potentials ranging -40 to $+70$ mV, after inactivation of I_{Na} .

The extracellular solution contained in mM: 140 NaCl, 5.4 KCl, 1.4 $CaCl_2$ (1.8 for human atrial myocytes), 1.2 $MgCl_2$, 10 glucose, 5 HEPES, 0.5 $CdCl_2$ (pH adjusted to 7.4 using NaOH). The pipette solution contained in mM: 120 K-aspartate; 20 KCl, 5 Na_2ATP , 2 $MgCl_2$, 5 EGTA, 10 HEPES (pH adjusted to 7.2 using KOH; pCa 7.0).

I_{KI} was obtained by digital subtraction of current traces, recorded with a ramp pulse from -100 to $+40$ mV, in the presence or absence of 1 mmol/L $BaCl_2$ (16) at room temperature (22 $^{\circ}C$), as described previously (37). The extracellular solution contained in mM: 120 NaCl, 20 KCl, 1 $MgCl_2$, 1.8 $CaCl_2$, 10 glucose, 10 HEPES, pH=7.4. High extracellular K^+ was used to shift the reversal potential to more positive values to obtain larger inward currents (37). The pipette solution contained in mM: 80 K-aspartate, 8 NaCl, 40 KCl, 2 $CaCl_2$, 5 Mg-ATP, 2 EGTA, 0.1 GTP-Tris, HEPES 10, pH=7.4

(ii) Recording of the L-type Ca^{2+} current.

Recording of $I_{Ca,L}$ was performed using a step-depolarization protocol (test potentials in the range -50 to $+50$ mV in 10 mV increments from a holding potential of -40 mV), as described previously (36). $I_{Ca,L}$ was measured as the difference between the current measured at the end of 250 ms test pulse and the peak inward current.

In vivo transesophageal burst pacing. AF inducibility was assessed in isoflurane (2%)-

anaesthetized mice by transesophageal burst pacing, as described previously (17). Briefly, a 1.7F catheter was advanced into the esophagus to capture the atria and deliver the electrical stimuli. Two pairs of intradermal electrodes were implanted to monitor ECG signals throughout the experiment. All electrical signals were pre-amplified and recorded using the Spike 2 software (version 7.09). Each burst was composed of 40 external stimulations at 1.5 times the threshold for atrial capture, starting from a cycle length of 60 ms and decreasing at each successive burst by 2 ms down to a final cycle length of 10 ms. Series of 25 bursts were repeated 3 times in each animal. An AF episode was defined as a period of rapid irregular atrial rhythm lasting at least 2 s.

***In silico* modeling.** Simulation studies were conducted using a population of virtual human atrial models based on the Maleckar *et al.* model (38), which yields an AP morphology closely resembling the human atrial APs recorded in this study. The model incorporates biophysically-detailed descriptions of the main transmembrane ionic currents, ion homeostasis and intracellular Ca^{2+} handling of the human atrial myocyte. Briefly, an initial population of 30,000 human atrial models was generated as in (15). For every model within the initial cell population, simulations were conducted using voltage clamp protocols and stimulation trains of 100 beats at five pacing frequencies (0.25, 0.5, 1, 2, 3 Hz) using identical protocols, as in the patch clamp experiments. Electrophysiological properties were calculated for each model at all pacing frequencies, including the magnitude of each ionic current as measured in voltage clamp, AP amplitude, APD_{50} and APD_{90} , AP triangulation and resting membrane potential. From the initial 30,000 sampled models, the experimentally-calibrated population of human atrial models was constructed by retaining only the models yielding values for all ionic currents and AP properties within the range obtained experimentally in SR. The resultant experimentally-calibrated SR population consisted of 640 human atrial models. The SR population was used to investigate the role of SMTC-induced changes in I_{to} , I_{Kur} , $I_{\text{Ca,L}}$ and I_{K1} in recovering APD changes measured experimentally.

Statistical analysis. The Student *t* test or the Mann-Whitney *U* test was used in 2-group comparisons. Multiple groups of normally distributed data of similar variance were compared by 1- or 2-way ANOVA, in some cases, after log transformation. For multiple comparisons, the Bonferroni's corrected P value is shown. The Kruskal-Wallis test or Wilcoxon test was used when the normality assumption was not met. Categorical variables were compared by χ^2 test; the Fisher exact test was used to compare surgical procedures. All statistical analysis was performed using GraphPad PRISM V5 or V6.04. Results are shown as mean \pm SEM or median and 95% confidence intervals or interquartile range, as appropriate. A value of $P < 0.05$ was considered statistically significant.

SUPPLEMENTARY MATERIAL

Fig. S1. Protein content of NOS isoforms in human and goat atrial tissue.

Fig. S2. Effect of nNOS knock-down and I_{Kur} inhibition on APD in human atrial myocytes.

Fig. S3. The atrial content of dystrophin and dystrophin-associated proteins is reduced in AF.

Fig. S4. Expression of atrial miR-31 under basal condition and following treatment with a miR-31-5p hairpin inhibitor (α -miR-31) in patients in AF or SR.

Fig. S5. Atrial miR-31, dystrophin and nNOS in patients in SR who developed AF after cardiac surgery and in those with paroxysmal AF.

Fig. S6. Reporter assay with dystrophin and nNOS sensors.

Fig. S7. Argonaute 2 (Ago2) and miR-31 content in Ago2 immunoprecipitates and effects of a miR-31 overexpression on dystrophin and nNOS, and on the electrical properties of atrial myocytes from patients in SR.

Table S1. Action potential characteristics of human and murine right atrial myocytes.

Table S2. *In vivo* cardiac electrophysiological parameters of WT and nNOS^{-/-} mice.

Table S3. Clinical and demographic characteristics of patients with paroxysmal atrial fibrillation and sinus rhythm controls.

Table S4. Clinical and demographic characteristics of patients in sinus rhythm before and after surgery and of those who developed postoperative atrial fibrillation.

Table S5. Predicted conserved (site 1) and poorly conserved (sites 2, 3, 4 and 5) miR-31 binding sites on the human nNOS 3'UTR.

Table S6. Sequences of the miR-31-5p mimic, miR-31-5p hairpin inhibitor (α -miR-31), target site blockers (TSB) and negative controls with the binding sites for miR-31 on the human dystrophin (DYS) and nNOS (site 5) 3'UTR.

REFERENCES

1. C. T. January, L. S. Wann, J. S. Alpert, H. Calkins, J. E. Cigarroa, J. C. Cleveland, Jr., J. B. Conti, P. T. Ellinor, M. D. Ezekowitz, M. E. Field, K. T. Murray, R. L. Sacco, W. G. Stevenson, P. J. Tchou, C. M. Tracy, C. W. Yancy, 2014 AHA/ACC/HRS guideline for the management of patients with atrial fibrillation: a report of the American College of Cardiology/American Heart Association Task Force on Practice Guidelines and the Heart Rhythm Society. *J Am Coll Cardiol* **64**, e1-76 (2014).
2. S. S. Chugh, R. Havmoeller, K. Narayanan, D. Singh, M. Rienstra, E. J. Benjamin, R. F. Gillum, Y. H. Kim, J. H. McAnulty, Jr., Z. J. Zheng, M. H. Forouzanfar, M. Naghavi, G. A. Mensah, M. Ezzati, C. J. Murray, Worldwide epidemiology of atrial

- fibrillation: a Global Burden of Disease 2010 Study. *Circulation* **129**, 837-847 (2014).
3. S. M. Al-Khatib, N. M. Allen LaPointe, R. Chatterjee, M. J. Crowley, M. E. Dupre, D. F. Kong, R. D. Lopes, T. J. Povsic, S. S. Raju, B. Shah, A. S. Kosinski, A. J. McBroom, G. D. Sanders, Rate- and rhythm-control therapies in patients with atrial fibrillation: a systematic review. *Ann Intern Med* **160**, 760-773 (2014).
 4. M. Allessie, J. Ausma, U. Schotten, Electrical, contractile and structural remodeling during atrial fibrillation. *Cardiovasc Res* **54**, 230-246 (2002).
 5. J. Tamargo, R. Caballero, R. Gomez, E. Delpon, Cardiac electrophysiological effects of nitric oxide. *Cardiovasc Res* **87**, 593-600 (2010).
 6. H. Cai, Z. Li, A. Goette, F. Mera, C. Honeycutt, K. Feterik, J. N. Wilcox, S. C. Dudley, Jr, D. G. Harrison, J. J. Langberg, Downregulation of Endocardial Nitric Oxide Synthase Expression and Nitric Oxide Production in Atrial Fibrillation: Potential Mechanisms for Atrial Thrombosis and Stroke. *Circulation* **106**, 2854-2858 (2002).
 7. A. Shiroshita-Takeshita, B. J. Brundel, B. Burstein, T. K. Leung, H. Mitamura, S. Ogawa, S. Nattel, Effects of simvastatin on the development of the atrial fibrillation substrate in dogs with congestive heart failure. *Cardiovasc Res* **74**, 75-84 (2007).
 8. J. C. Williams, A. L. Armesilla, T. M. Mohamed, C. L. Hagarty, F. H. McIntyre, S. Schomburg, A. O. Zaki, D. Oceandy, E. J. Cartwright, M. H. Buch, M. Emerson, L. Neyses, The sarcolemmal calcium pump, alpha-1 syntrophin, and neuronal nitric-oxide synthase are parts of a macromolecular protein complex. *J Biol Chem* **281**, 23341-23348 (2006).
 9. Y. H. Zhang, B. Casadei, Sub-cellular targeting of constitutive NOS in health and disease. *J Mol Cell Cardiol* **52**, 341-350 (2012).
 10. Z. Jian, H. Han, T. Zhang, J. Puglisi, L. T. Izu, J. A. Shaw, E. Onofriok, J. R. Erickson, Y. J. Chen, B. Horvath, R. Shimkunas, W. Xiao, Y. Li, T. Pan, J. Chan, T. Banyasz, J. C. Tardiff, N. Chiamvimonvat, D. M. Bers, K. S. Lam, Y. Chen-Izu, Mechanochemotransduction during cardiomyocyte contraction is mediated by localized nitric oxide signaling. *Science signaling* **7**, ra27 (2014).
 11. G. D. Thomas, M. Sander, K. S. Lau, P. L. Huang, J. T. Stull, R. G. Victor, Impaired metabolic modulation of alpha-adrenergic vasoconstriction in dystrophin-deficient skeletal muscle. *Proc Natl Acad Sci U S A* **95**, 15090-15095 (1998).
 12. M. Seddon, N. Melikian, R. Dworakowski, H. Shabeeh, B. Jiang, J. Byrne, B. Casadei, P. Chowienzyk, A. M. Shah, Effects of neuronal nitric oxide synthase on human coronary artery diameter and blood flow in vivo. *Circulation* **119**, 2656-2662 (2009).
 13. J. E. Brenman, D. S. Chao, H. Xia, K. Aldape, D. S. Brecht, Nitric oxide synthase complexed with dystrophin and absent from skeletal muscle sarcolemma in Duchenne muscular dystrophy. *Cell* **82**, 743-752 (1995).
 14. M. Sander, B. Chavoshan, S. A. Harris, S. T. Iannaccone, J. T. Stull, G. D. Thomas, R. G. Victor, Functional muscle ischemia in neuronal nitric oxide synthase-deficient skeletal muscle of children with Duchenne muscular dystrophy. *Proc Natl Acad Sci U S A* **97**, 13818-13823 (2000).
 15. O. J. Britton, A. Bueno-Orovio, K. Van Ammel, H. R. Lu, R. Towart, D. J. Gallacher, B. Rodriguez, Experimentally calibrated population of models predicts and explains intersubject variability in cardiac cellular electrophysiology. *Proc Natl Acad Sci U S A* **110**, E2098-2105 (2013).
 16. Z. Wang, B. Fermini, S. Nattel, Sustained depolarization-induced outward current in human atrial myocytes. Evidence for a novel delayed rectifier K⁺ current similar to Kv1.5 cloned channel currents. *Circ Res* **73**, 1061-1076 (1993).
 17. S. Verheule, T. Sato, T. t. Everett, S. K. Engle, D. Otten, M. Rubart-von der Lohe, H. O. Nakajima, H. Nakajima, L. J. Field, J. E. Olgin, Increased vulnerability to atrial fibrillation in transgenic mice with selective atrial fibrosis caused by overexpression of TGF-beta1. *Circ Res* **94**, 1458-1465 (2004).

18. Y. Lai, G. D. Thomas, Y. Yue, H. T. Yang, D. Li, C. Long, L. Judge, B. Bostick, J. S. Chamberlain, R. L. Terjung, D. Duan, Dystrophins carrying spectrin-like repeats 16 and 17 anchor nNOS to the sarcolemma and enhance exercise performance in a mouse model of muscular dystrophy. *J Clin Invest* **119**, 624-635 (2009).
19. W. J. Chang, S. T. Iannaccone, K. S. Lau, B. S. Masters, T. J. McCabe, K. McMillan, R. C. Padre, M. J. Spencer, J. G. Tidball, J. T. Stull, Neuronal nitric oxide synthase and dystrophin-deficient muscular dystrophy. *Proc Natl Acad Sci U S A* **93**, 9142-9147 (1996).
20. D. Cacchiarelli, T. Incitti, J. Martone, M. Cesana, V. Cazzella, T. Santini, O. Sthandier, I. Bozzoni, miR-31 modulates dystrophin expression: new implications for Duchenne muscular dystrophy therapy. *EMBO reports* **12**, 136-141 (2011).
21. N. Voigt, J. Heijman, Q. Wang, D. Y. Chiang, N. Li, M. Karck, X. H. Wehrens, S. Nattel, D. Dobrev, Cellular and molecular mechanisms of atrial arrhythmogenesis in patients with paroxysmal atrial fibrillation. *Circulation* **129**, 145-156 (2014).
22. G. Hutvagner, M. J. Simard, Argonaute proteins: key players in RNA silencing. *Nat Rev Mol Cell Biol* **9**, 22-32 (2008).
23. X. Luo, B. Yang, S. Nattel, MicroRNAs and atrial fibrillation: mechanisms and translational potential. *Nat Rev Cardiol* **12**, 80-90 (2015).
24. D. Cacchiarelli, J. Martone, E. Girardi, M. Cesana, T. Incitti, M. Morlando, C. Nicoletti, T. Santini, O. Sthandier, L. Barberi, A. Auricchio, A. Musaro, I. Bozzoni, MicroRNAs involved in molecular circuitries relevant for the Duchenne muscular dystrophy pathogenesis are controlled by the dystrophin/nNOS pathway. *Cell metabolism* **12**, 341-351 (2010).
25. N. Shirokova, E. Niggli, Cardiac phenotype of Duchenne Muscular Dystrophy: insights from cellular studies. *J Mol Cell Cardiol* **58**, 217-224 (2013).
26. S. N. Reilly, R. Jayaram, K. Nahar, C. Antoniadou, S. Verheule, K. M. Channon, N. J. Alp, U. Schotten, B. Casadei, Atrial sources of reactive oxygen species vary with the duration and substrate of atrial fibrillation: implications for the antiarrhythmic effect of statins. *Circulation* **124**, 1107-1117 (2011).
27. W. O. Idigo, S. Reilly, M. H. Zhang, Y. H. Zhang, R. Jayaram, R. Carnicer, M. J. Crabtree, J. L. Balligand, B. Casadei, Regulation of endothelial nitric-oxide synthase (NOS) S-glutathionylation by neuronal NOS: evidence of a functional interaction between myocardial constitutive NOS isoforms. *J Biol Chem* **287**, 43665-43673 (2012).
28. R. Gomez, L. Nunez, M. Vaquero, I. Amoros, A. Barana, T. de Prada, C. Macaya, L. Maroto, E. Rodriguez, R. Caballero, A. Lopez-Farre, J. Tamargo, E. Delpon, Nitric oxide inhibits Kv4.3 and human cardiac transient outward potassium current (Ito1). *Cardiovasc Res* **80**, 375-384 (2008).
29. R. Gomez, R. Caballero, A. Barana, I. Amoros, E. Calvo, J. A. Lopez, H. Klein, M. Vaquero, L. Osuna, F. Atienza, J. Almendral, A. Pinto, J. Tamargo, E. Delpon, Nitric Oxide Increases Cardiac IK1 by Nitrosylation of Cysteine 76 of Kir2.1 Channels. *Circ Res* **105**, 383-392 (2009).
30. U. Schotten, S. Verheule, P. Kirchhof, A. Goette, Pathophysiological mechanisms of atrial fibrillation: a translational appraisal. *Physiol Rev* **91**, 265-325 (2011).
31. E. van Rooij, A. L. Purcell, A. A. Levin, Developing microRNA therapeutics. *Circ Res* **110**, 496-507 (2012).
32. U. Schotten, M. Duytschaever, J. Ausma, S. Eijssbouts, H. R. Neuberger, M. Allesie, Electrical and contractile remodeling during the first days of atrial fibrillation go hand in hand. *Circulation* **107**, 1433-1439 (2003).
33. B. Cox, A. Emili, Tissue subcellular fractionation and protein extraction for use in mass-spectrometry-based proteomics. *Nat Protoc* **1**, 1872-1878 (2006).
34. L. Sartiani, P. De Paoli, G. Lonardo, R. Pino, A. A. Conti, E. Cerbai, A. Pelleg, L. Belardinelli, A. Mugelli, Does recombinant human interleukin-11 exert direct electrophysiologic effects on single human atrial myocytes? *J Cardiovasc Pharmacol* **39**, 425-434 (2002).

35. O. Ellingsen, A. J. Davidoff, S. K. Prasad, H. J. Berger, J. P. Springhorn, J. D. Marsh, R. A. Kelly, T. W. Smith, Adult rat ventricular myocytes cultured in defined medium: phenotype and electromechanical function. *Am J Physiol* **265**, H747-754 (1993).
36. C. E. Sears, S. M. Bryant, E. A. Ashley, C. A. Lygate, S. Rakovic, H. L. Wallis, S. Neubauer, D. A. Terrar, B. Casadei, Cardiac neuronal nitric oxide synthase isoform regulates myocardial contraction and calcium handling. *Circ Res* **92**, e52-59 (2003).
37. N. Voigt, A. Trausch, M. Knaut, K. Matschke, A. Varro, D. R. Van Wagoner, S. Nattel, U. Ravens, D. Dobrev, Left-to-right atrial inward rectifier potassium current gradients in patients with paroxysmal versus chronic atrial fibrillation. *Circ Arrhythm Electrophysiol* **3**, 472-480 (2010).
38. M. M. Maleckar, J. L. Greenstein, W. R. Giles, N. A. Trayanova, K⁺ current changes account for the rate dependence of the action potential in the human atrial myocyte. *Am J Physiol Heart Circ Physiol* **297**, H1398-1410 (2009).

Acknowledgements: We would like to thank Dr Andrew Jefferson and Dr Janet Digby for their assistance in conducting immunofluorescence experiments and Dr Kevin Clark for his help with FACS experiments and analysis.

Funding: This study was funded by a British Heart Foundation (BHF) Programme Grant (RG/11/15/29375) to BC, the Oxford BHF Centre of Excellence (RE/13/1/3018) (SR, RW) and, in part, by a Fondation Leducq Network of Excellence (08CVD01) (BC, SR, MS), the European Union 7th Framework Programme under Grant Agreement n°261057 (EUTRAF) (BC, RC), an FP7 Marie Curie (ITN) grant (RADOX) to MCC, and a Wellcome Trust studentship to OL (099898/Z/12/Z).

TAF and TR are funded by a WIMM strategic award and the UK Medical Research Council (#G0902418). BR is supported by a Wellcome Trust Senior Research Fellowship (100246/Z/12/Z). AM holds an EPSRC scholarship from the Systems Biology Doctoral Training Centre of the University of Oxford.

Author contributions: BC and SR conceived the study, designed the experiments and wrote the manuscript. SR and XL carried out and analyzed most of the experimental work with the exception of *in vivo* experiments in the mouse (performed by RC and AR). AM, AB-O and BR carried out the in-silico simulation study. US and SV provided tissue samples from the goat atrial fibrillation model and supervised *in vivo* experiments in the mouse. RW, OL, RJ, CR, RS, GK, NS, MCC and MS were involved in consenting patients, collecting and processing human atrial tissue samples, and isolating and culturing human atrial myocytes. TAF and TR designed the miR-31 reporter assays. All authors had the opportunity to discuss the results and contribute to the manuscript.

Competing interests: BC and SR hold a UK patent related to this work.

Figure Legends

Figure 1. Loss of atrial nNOS in AF contributes to atrial electrical remodelling.

Atrial NOS activity and nNOS protein are significantly reduced in right atrial (RA) tissue (**A**) and myocytes (**B**) from patients with AF (N=17 vs. SR, N=19 and N=12 vs. SR, N=19, respectively) and in goats (**C, D**) after 2 weeks (2W, N=6-7) or 6 months (6M, N=7-8) of AF vs. SR (N=9-11). (**A**) *right panel*: representative chromatograms showing lower L-citrulline production, *i.e.*, reduced NO synthesis, in AF and average data (*left panel*).

+, murine brain is the positive control for nNOS. LA, left atrium.

In RA myocytes from patients in SR (**E, F**), nNOS inhibition with SMTC shortens APD₉₀ (SMTC: n=45/N=12 vs. vehicle: n=52/N=14) and abolishes APD₉₀ rate-dependent adaptation (SMTC: n=22/N=7 vs. vehicle: n=39/N=11; $P<0.01$ for the interaction between rate and treatment); by contrast, SMTC had no effect on APD₉₀ in AF (**E, F**; SMTC, n=40/N=13 vs. vehicle, n=27/N=6).

nNOS inhibition or gene deletion shortens APD₉₀ in murine right atrial myocytes. SMTC has no effect on APD in atrial myocytes from nNOS^{-/-} mice (**G**; SMTC: n=9/N=4; nNOS^{-/-}: n=28/N=9; WT: n=18/N=6).

N, number of patients/animals; n, number of cells. * $P<0.05$, ** $P<0.01$, *** $P<0.001$ vs. SR or WT mice, # $P<0.05$, ## $P<0.01$, ### $P<0.001$ vs. vehicle or between LA and RA, by unpaired *t* test (**A, B**), or 1-way ANOVA with Bonferroni correction in (**C, E, G**), or Kruskal-Wallis test (**D**) and by 2-way repeated measures ANOVA with Bonferroni correction (**F**).

Figure 2. nNOS disruption increases repolarizing K⁺ currents and promotes AF inducibility *in vivo* in mice.

(**A**) Peak (I_{to}) and sustained (I_{sus}) ion currents elicited with the voltage protocol illustrated at the top in right atrial myocytes from patients in SR, (**B**) mean current–voltage relationships of the 4-aminopyridine (4-AP)-sensitive I_{Kur} and (**C**) I_{K1} in the presence or absence of nNOS inhibition with SMTC.

(**D**) Simulation of the effect of the changes ion currents elicited by SMTC on human atrial AP. (**E**) In an *in silico* population of human atrial SR models (n=640), the increase in I_{Kur} elicited by SMTC reproduced the shortening in APD₅₀ whereas the combined increase in I_{Kur} and I_{K1} recovered all APD changes recorded in the presence of SMTC. The recorded differences in I_{Ca} and I_{to} had virtually no impact on APD.

(**F**) Representative ECG traces following atrial burst pacing in anesthetized mice (*left*) and mean data (*right*) on AF probability and duration of the induced AF episodes in WT (N=19) and nNOS^{-/-} mice (N=18).

N, number of patients/mice, n=cells/models; (**B, C**) ## $P<0.01$ and ### $P<0.001$ for the interaction between voltage and SMTC (2-way repeated measure ANOVA with Bonferroni correction). (**f**) * $P<0.05$ between genotypes by Mann-Whitney *U* test. Non-normally distributed data are shown as box plots (median and 95% CI).

Figure 3. Atrial myocyte-specific increase in miR-31 expression in AF is associated with a reduction in dystrophin and nNOS.

(A, B) Immunostaining (N=4/group), (C) immunoprecipitation (N=5/group) and (D) immunoblotting of the membrane (M) & cytosolic (C) fraction (N=4/group) of right atrial tissue or myocytes from patients with AF show loss of dystrophin (DYS) and nNOS co-localization at the sarcolemmal membrane. Scale bar, 20 μ m.

In human (E) and goat atrial tissue (Figure S3A, B), atrial dystrophin (DYS) and its associated proteins, caveolin-3 (Cav-3) and α 1 syntrophin (α 1 SYN), are significantly reduced in the presence of AF (N=10) vs. SR (N=9). Protein expression is normalized to GAPDH.

(F) nNOS mRNA is significantly lower in atrial myocytes from patients with AF (N=7 vs. SR: N=8), whereas (G) dystrophin mRNA is unchanged (N=13 vs. SR: N=18).

(H) miR-31 expression is significantly higher in human right atrial myocytes in the presence of AF, (N=17 vs. SR: N=19) and (I) in goat left atrial (LA) tissue (N=7 vs. SR: N=11). In the goat left ventricle (LV), miR-31 expression in SR is significantly lower than in the LA, and is unchanged by AF (I).

N, number of patients/animals. *P<0.05, **P<0.01 vs. SR or #P<0.05, ###P<0.001 vs. LV by Mann-Whitney *U* test (B, G, H) or by unpaired t-test (E, F) and by 1-way ANOVA with Bonferroni correction (I). Non-normally distributed data are shown as median and interquartile range. Transcripts were normalized to GAPDH (dystrophin and nNOS) or snoU6 (miR-31) and related to a control reference sample

Figure 4. miR-31 targets dystrophin and nNOS mRNA.

In atrial myocytes from patients with AF, selective protection of the miR-31 binding site on dystrophin (A, DYS, N=7-9) or nNOS (B, N=7-9) mRNA (TSB, striped columns) selectively prevents loading of the respective mRNA on the RISC in Argo-2 immunoprecipitates. nNOS and dystrophin mRNA was normalized to miR-31 (see also Fig. S7B).

In actinomycin D-treated atrial myocytes from patients in SR, a miR-31 mimic accelerates the rate of decay of nNOS mRNA (C, N=4/group), but not of dystrophin mRNA (D, N=4/group, blue circles vs. NC – black squares). nNOS and dystrophin mRNA was normalized to GAPDH and expressed as a percentage of the respective mRNA at 0 hour.

In atrial myocytes from patients with AF, preventing miR-31 binding to the nNOS mRNA 3'UTR with the nNOS-TSB (striped columns) increases nNOS mRNA (E) and protein level (F, N=5-8) but does not affect dystrophin (DYS, N=5-8). By contrast, transfection with DYS-TSB has no effect on either DYS or nNOS mRNA (G), but significantly increases the protein level of both (H, N=5).

N, number of patients; NC, negative non-targeting control for TSB (Exiqon) and negative non-targeting control #1 for miR-31 mimic (Dharmacon); T, TSB treatment.

#P<0.05, ###P<0.01, ####P<0.001 vs. NC by Wilcoxon matched pairs test (A), or paired t test (B), or by 2-way ANOVA with Bonferroni correction (C, D), or by unpaired *t* test (E, H and F, G for dystrophin only) and by Mann-Whitney *U* test (F, G – for nNOS). Non-normally distributed data are shown as median and interquartile range.

Figure 5. Inhibition of miR-31 recovers nNOS and dystrophin and restores APD in AF.

In atrial myocytes from patients with AF (**A**, **B**), treatment with a miR-31 hairpin inhibitor (α -miR-31) restores nNOS mRNA and protein (N=5-6 and N=9 per group, i.e., NC and α -miR-31) and dystrophin (DYS) protein without affecting DYS mRNA (**B**, N=5-9/group).

By contrast, in SR (**C-D**), α -miR-31 does not affect the protein or mRNA content of dystrophin (protein: N=7/group, mRNA: N=6/group) or nNOS (protein: N=5-6; mRNA: N=4-5/group).

In atrial myocytes from patients with AF (n=12/N=3/group), α -miR-31 also restores APD₉₀ (**E**, *left*: raw data traces; *right*: mean values) and APD₉₀ rate-dependent adaptation (**F**); both effects are abolished after nNOS inhibition with SMTC (**E**, **F**, n=11/N=3).

(**G**) Summary diagram of the main findings: atrial miR-31 upregulation in human AF accelerates nNOS mRNA decay and alters nNOS subcellular localization and protein stability by inhibiting dystrophin translation. The resulting reduction in nNOS-derived NO contributes to the AF-induced electrical remodeling and, thus, to the maintenance and progression of AF.

N, number of patients; n, number of cells. NC, negative non-targeting control #1 (Dharmacon).

#P<0.05, ##P<0.01, ###P<0.001 vs. NC by paired t test (**A**), or unpaired *t* test (**B-D** – for nNOS), or Mann-Whitney *U* test (**D** –for dystrophin), and by 1- (**E**) or 2-way repeated measures ANOVA (**F**) with Bonferroni correction. Non-normally distributed data are expressed as median with interquartile range.

Groups of comparison	SR	Persistent AF
Total number of patients	176	51
Age, years (mean±SD)	69±10	72±10
Men, N and (%)	123 (70)	33 (65)
Surgical procedure, N and (%)		
CABG±AVR/MVR	125 (71)	17 (33) *
AVR/MVR	51 (29)	27 (53)
Maze procedure	0 (0)	7 (14) ***
Medical history, N and (%)		
Smoker/ex-smoker	99 (56)	21 (41)
Hypertension	130 (74)	31 (61)
Diabetes mellitus	39 (22)	6 (12)
Heart Failure	42 (24)	18 (35)
Previous MI	55 (31)	2 (4)**
COPD/asthma	12 (7)	6 (12)
Medications, N and (%)		
Anticoagulants	16 (9)	33 (64) ***
Antiplatelets	127 (72)	11 (22)**
β-blockers	100 (57)	23 (45)
Statins	128 (73)	25 (49)
CCB	35 (20)	6 (12)
ACEIs and ARBs	97 (55)	22 (43)
Diuretics	48 (27)	22 (43)

Table 1. Clinical and demographic characteristics of patients in sinus rhythm and with persistent atrial fibrillation.

%, percent of total in each group. SR, sinus rhythm; AF, atrial fibrillation; CABG, coronary artery bypass surgery; AVR, aortic valve replacement; MVR, mitral valve replacement; MI, myocardial infarction; COPD, chronic obstructive pulmonary disease; CCB, calcium channel blocker; ACEI, angiotensin-converting enzyme inhibitor, and ARB, angiotensin II receptor blocker.

* $P < 0.05$, ** $P < 0.01$, *** $P < 0.001$ vs. patients in SR, by χ^2 test for gender, smoking status, and medical history, by the Fisher's exact test for surgical procedures and by unpaired t test for age.

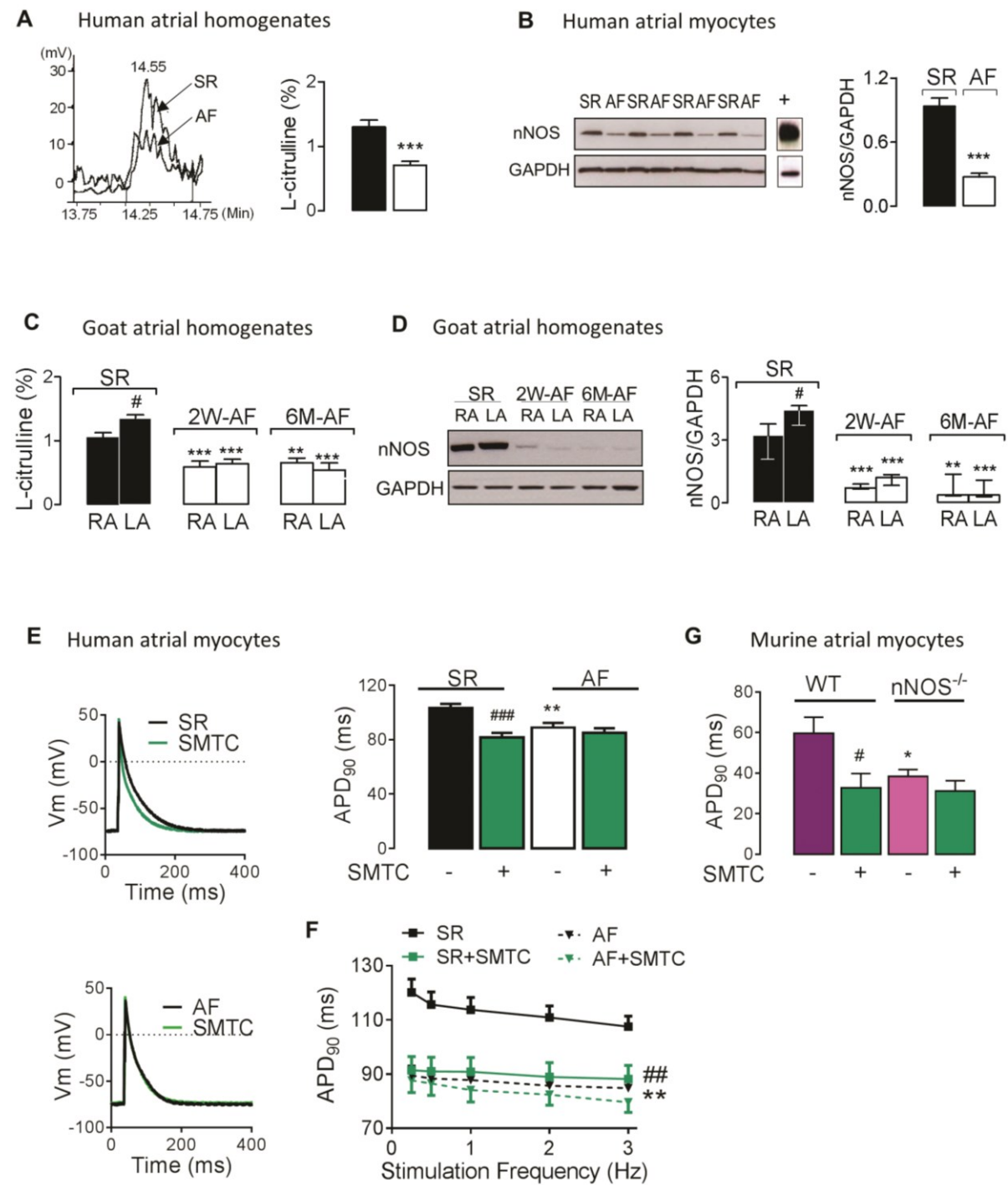
Figure 1

Figure 2

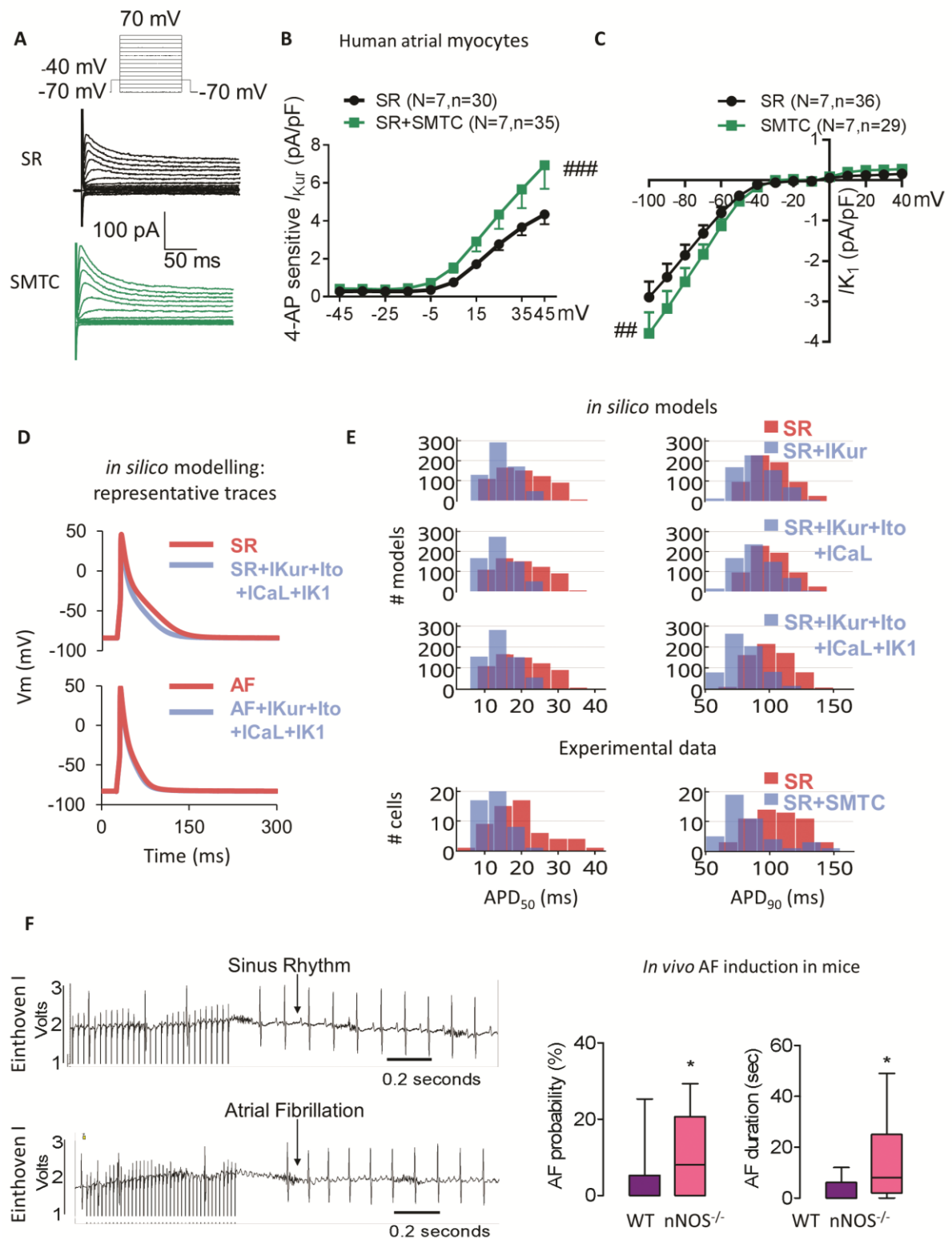


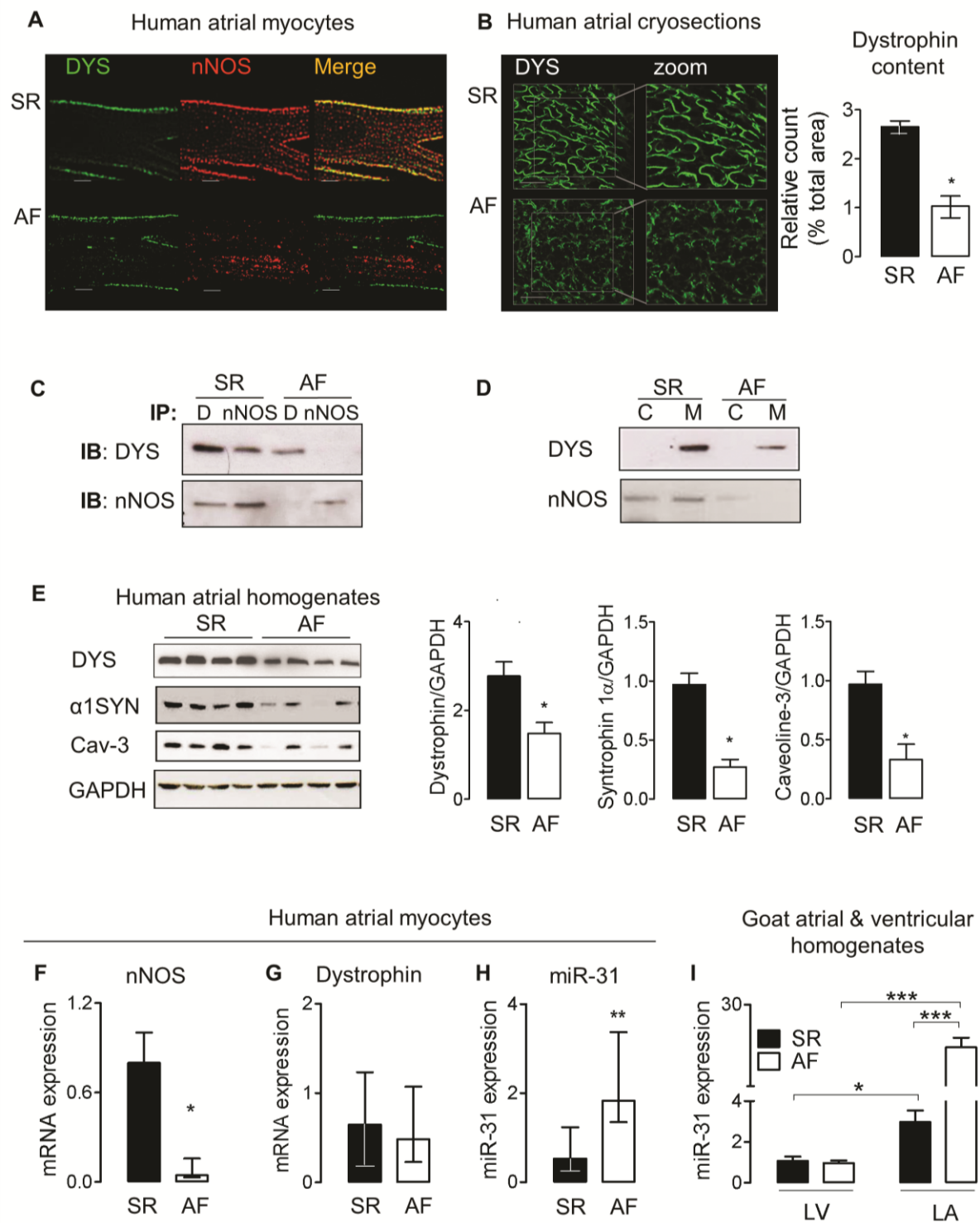
Figure 3

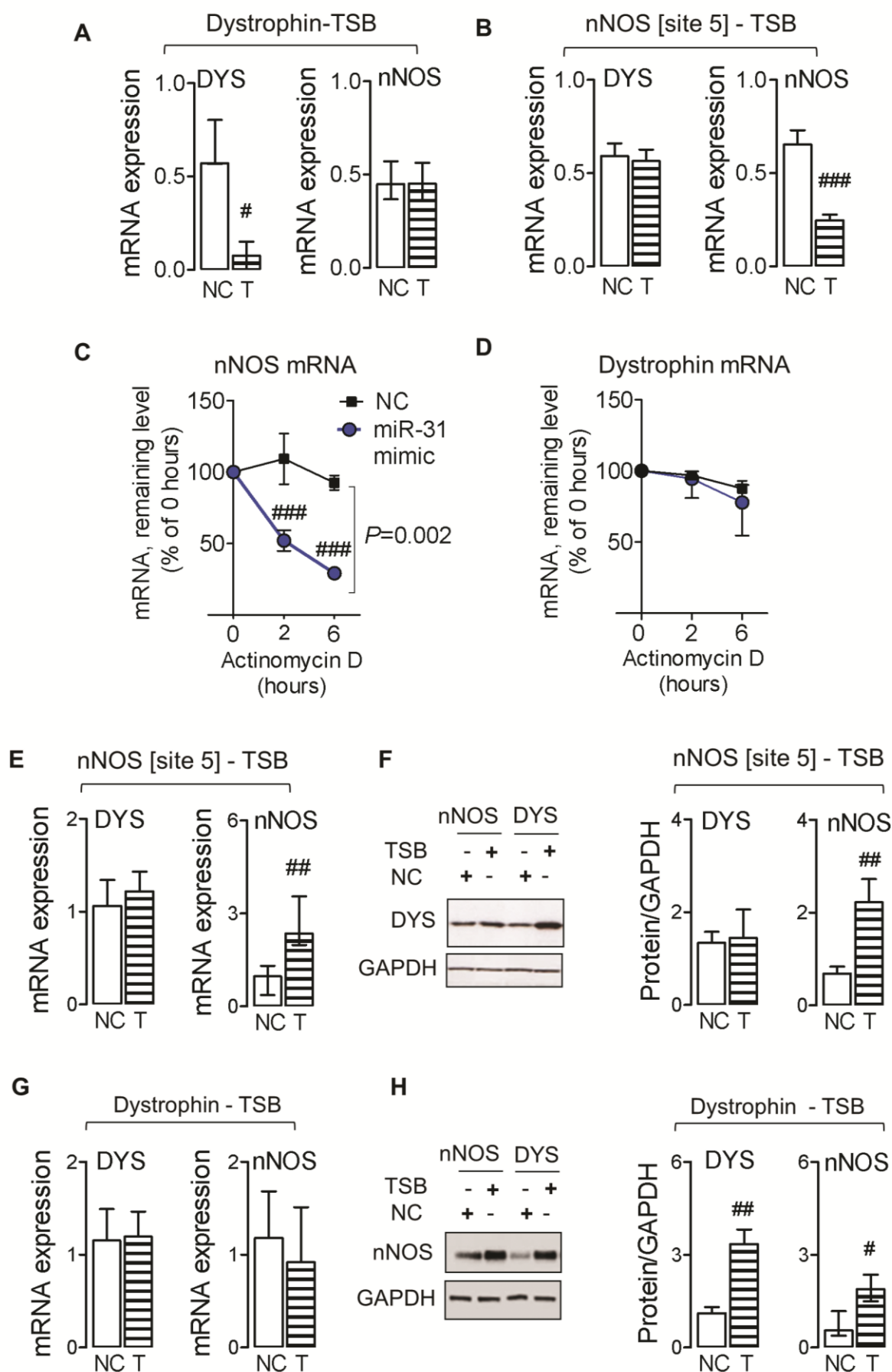
Figure 4

Figure 5